



Supporting Information

© Wiley-VCH 2008

69451 Weinheim, Germany

Supporting Information

Effects of Guanidinium-Phosphate Hydrogen Bonding on the Membrane-Bound Structure and Activity of an Arginine-Rich Membrane Peptide from Solid-State NMR

Ming Tang¹, Alan J. Waring², Robert I. Lehrer², and ¹

¹ Department of Chemistry, Iowa State University, Ames, IA 50011

² Department of Medicine, University of California at Los Angeles, Los Angeles, CA

90095

Antimicrobial assays

Radial diffusion assays were performed in media supplemented with 100 mM NaCl or in low salt media. Both assay media contained 10 mM sodium phosphate buffer, 1% agarose, and 0.3 mg/ml of trypticase soy broth powder to allow the organisms to grow until the underlay assay gel was covered with a nutrient-rich overlay gel that allowed surviving microbes to form colonies. The high-salt results are more predictive of activity in physiological fluids.

Table S1. Minimum effective concentrations (MEC) of PG-1 and Arg^{mmm}-PG-1 against various bacteria at high and low salt conditions.

MEC ($\mu\text{g/ml}$)	100 mM NaCl		Low NaCl	
	PG-1	Arg ^{mmm} -PG-1	PG-1	Arg ^{mmm} -PG-1
Gram-negative bacteria				
<i>E. coli</i>	1.09	3.00	1.55	1.58
<i>P. aeruginosa</i>	1.39	3.41	1.90	1.62
<i>K. pneumoniae</i>	1.93	8.76	4.47	7.9
Gram-positive bacteria				
<i>S. epidermidis</i>	1.07	1.90	4.19	4.29
<i>E. faecalis</i>	1.54	3.10	4.10	3.17
<i>B. subtilis</i>	1.22	3.91	1.79	3.58
<i>S. aureus</i>	1.66	10.4	5.10	9.35
mean (n=7)	1.41	4.92	3.30	4.50

The mean activities of PG-1 and Arg^{mmm}-PG-1 in 100 mM NaCl differ significantly ($p < 0.001$ by the Mann-Whitney Rank Sum test).

Table 1 shows that higher salt concentration increases the activity of PG-1, but does not affect the activity of Arg^{mmm}-PG-1. We hypothesize that higher salt concentration promotes PG-1 aggregation, which is essential for its toroidal-pore mechanism of action^[2]. In our previous study of the structure of PG-1 fibrils outside the lipid membrane,^[1]

high salt concentration was used to promote fibril formation. The fact that salt level does not affect the activity of Arg^{mm}-PG-1 suggests that the mutant adopts a different mechanism of action that does not require peptide aggregation. This is consistent with the large-amplitude dynamics observed for the mutant.

Motionally averaged dipolar couplings and chemical shift anisotropies

C-H dipolar couplings of Arg^{mm}-PG-1 were measured using the 2D LG-CP experiment^[3] for the POPC/POPG sample and the DIPSHIFT experiment^[4] for the POPE/POPG sample. The LG-CP experiment was conducted under 10 kHz spinning at 295 K. The DIPSHIFT experiment was performed under 3.5 kHz MAS at 303 K, the higher temperature due to the higher phase transition temperature of the POPE/POPG membrane. The MREV-8 sequence was used for ¹H homonuclear decoupling. The scaling factors for the LG-CP sequence and the MREV-8 sequence are 0.57 and 0.47, respectively.

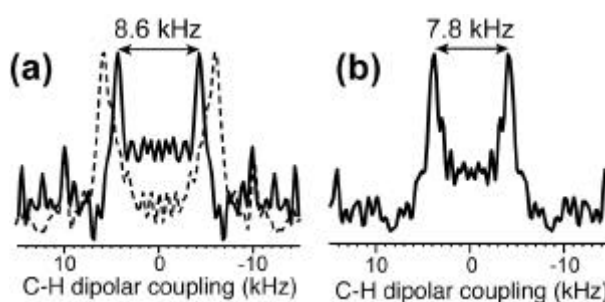


Fig. S1. ¹³C-¹H LG-CP cross sections of Arg^{mm}-PG-1 in the POPC/POPG membrane at 295 K. (a) L5 Cα. (b) V14 Cα. Dashed line in (a) indicates the rigid-limit coupling of 12.5 kHz, measured at 233 K. The experimental uncertainty is ±0.2 kHz.

In addition to C-H dipolar couplings, we measured the C α chemical shift anisotropy (CSA) of L5 and V14 using the ROCSA experiment^[5] to assess if the backbone motion is uniaxial. The experiment was carried out at 303 K on the POPE/POPG membrane samples under 6 kHz MAS. Fig. S2 shows the ROCSA spectra and the relevant peptide and lipid cross sections. The lipid cross sections (Fig. S2c) give a control of the expected uniaxial lineshapes due to the known uniaxial rotation of lipids around the bilayer normal. It can be seen that the peptide L5 and V14 C α sites also have uniaxial lineshapes (Fig. S2b), with motionally narrowed anisotropy parameter $\bar{\delta}$ of 17 ppm for L5 and 11 ppm for V14. The rigid-limit anisotropy parameter δ for β -sheet Val is known from previous experimental studies to be 25 ppm^[6], while the rigid-limit δ for the β -sheet conformation of Leu has been obtained from *ab initio* calculations to be 19.5 ppm^[7]. Thus, the CSA order parameter $S_{\text{CSA}} = \bar{\delta}/\delta$ is 0.89 for L5 and 0.44 for V14. These values are consistent with the C-H order parameters measured for these two sites in the POPE/POPG membrane. Most importantly, the uniaxial CSA lineshapes confirm the presence of uniaxial rotation of the Arg^{mm}-PG-1 backbone around the membrane normal.

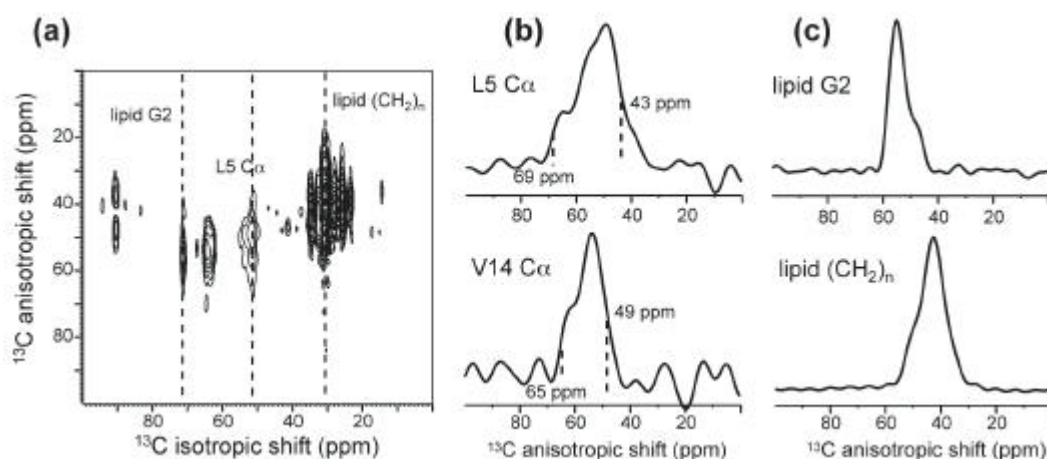


Fig. S2. $^{13}\text{C}\alpha$ CSA of Arg^{mmm}-PG-1. (a) 2D ROCSA spectra of Arg^{mmm}-PG-1 in POPE/POPG membranes at 303 K. (b) 1D cross sections of the peptide L5 and V14 C α sites. (c) 1D cross sections of two lipid peaks, glycerol G2 and acyl chain (CH₂)_n. The lipid lineshapes are uniaxial as expected. The peptide lineshapes are similarly uniaxial, indicating uniaxial rotation around the membrane normal.

Orientation calculations

The ideal antiparallel β -hairpin structure was constructed using (ϕ , ψ) torsion angles of (-137°, +135°) for the strand residues, and (-45°, +85°) and (+155°, -20°) for the $i+1$ and $i+2$ residues of the β -turn^[8]. The turn torsion angles were modified from the classical β -turn conformations to make the two strands approximately parallel. The strand axis was chosen to be the average orientation of six consecutive C'-N bonds from residue 4 to residue 9. The tilt angle τ is the angle between this strand axis and the bilayer normal. The ρ angle was defined as the angle between the C=O bond of residue 6 and the common plane of the strand axis and the bilayer normal. The peptide was rotated through all combinations of (τ , ρ) angles and the C-H dipolar couplings of the N-strand residues 4 - 8 and C-strand residues 13 - 17 were calculated and converted to the order parameter according to $S_{\text{CH}} = \omega(\tau, \rho) / \omega_{\text{rigid}}$.

Fig. S3 shows a more extended set of S_{CH} values for (τ , ρ) angles in the range (10-90°, 0°-180°), which complements the simulations in Fig. 5. The best fit (τ , ρ) in this range for the POPE/POPG bound Arg^{mmm}-PG-1 is (64°, 359°), and is related to the global best fit (116°, 179°) by symmetry.

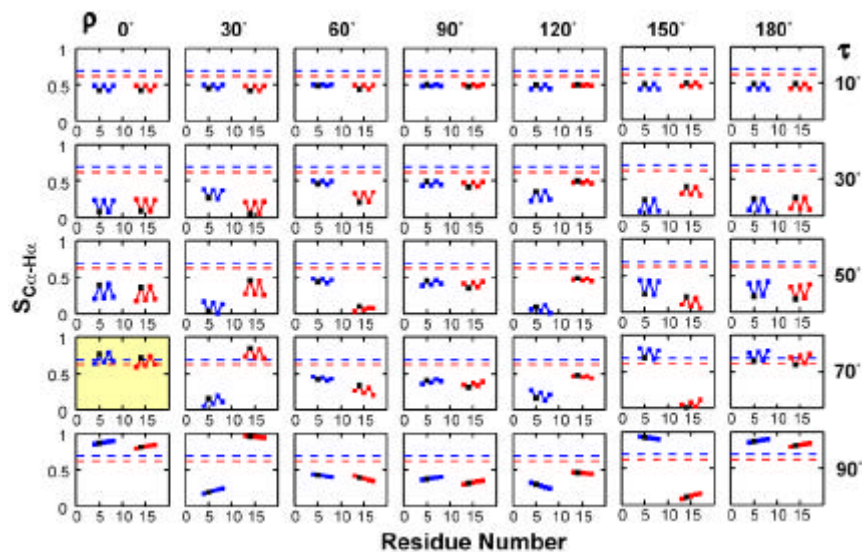


Fig. S3. S_{CH} of an ideal β -hairpin as a function of (τ, ρ) . The N- and C-strand S_{CH} 's are plotted as blue and red squares, respectively, with the L5 and V14 values in black. The experimental S_{CH} 's for L5 and V14 in the POPC/POPG membrane are drawn as blue and red dashed lines. The yellow highlighted panel indicates the approximate position of one of the four best-fit orientations.

Fig. S4 shows the RMSD between the calculated S_{CH} and the experimental S_{CH} 's of L5 and V14 in the POPC/POPG membrane. The RMSD is calculated as

$$\text{RMSD} = \sqrt{\left(S_{CH,calc}^{L5} - S_{CH,exp t}^{L5} \right)^2 + \left(S_{CH,calc}^{V14} - S_{CH,exp t}^{V14} \right)^2}.$$

From the RMSD, four symmetry-related best-fit orientations are identified and listed in Table S2. Taking into account the ^{13}C - ^{31}P distance constraints, the global best-fit (τ, ρ) angles are orientation A, $(116^\circ, 179^\circ)$.

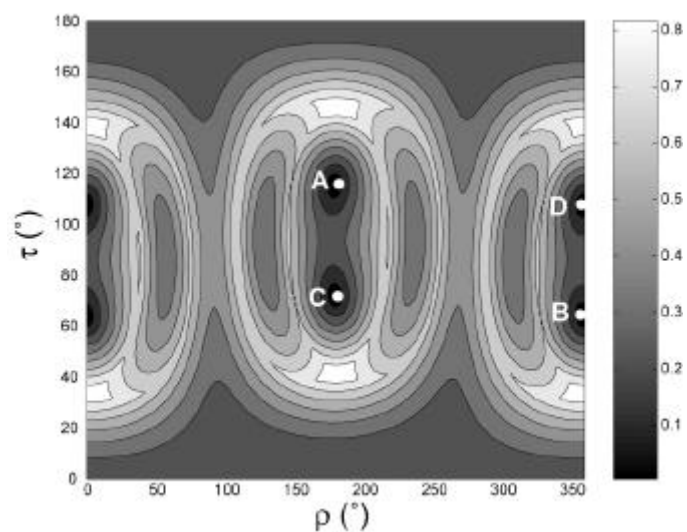


Fig. S4. RMSD between the calculated and experimental $C\alpha$ - $H\alpha$ order parameters of Arg^{mm} -PG-1 in the POPC/POPG membrane as a function of (τ, ρ) . The four lowest RMSD positions are related by symmetry and are indicated as A, B, C, D.

To obtain the peptide orientation in the POPE/POPG membrane, we carried out the same S_{CH} calculation but compared these with the POPE/POPG experimental data. Fig. S5a shows S_{CH} for (τ, ρ) of $(50-130^\circ, 160^\circ-340^\circ)$. The ideal β -hairpin structure is used in the calculation. Again, four symmetry-related best-fit orientations are found according to the RMSD analysis (Fig. S5b). The orientation $(\tau, \rho) = (113^\circ, 164^\circ)$ is chosen as the global best fit because it agrees best with the ^{13}C - ^{31}P distance data. This orientation is quite similar to that found in POPC/POPG membranes, as shown by the schematic representation in Fig. S5c, indicating that the composition change from POPC to POPE lipids does not affect the Arg^{mm} -PG-1 orientation significantly.

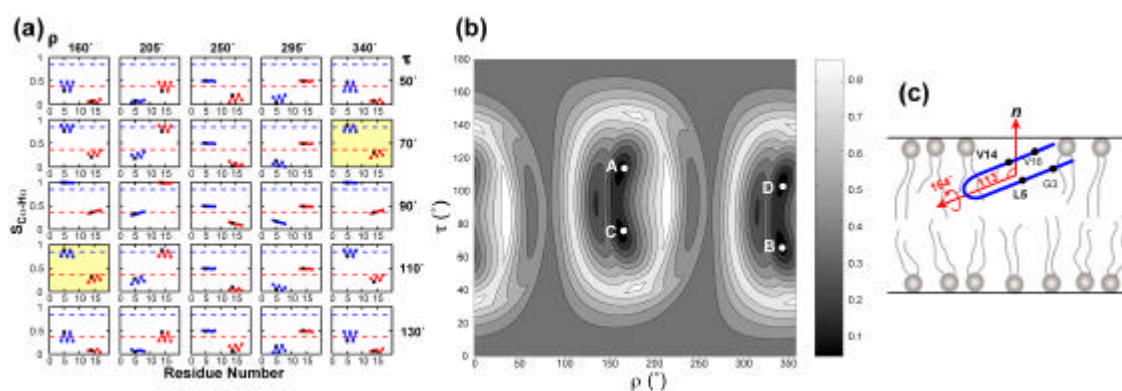


Fig. S5. Orientation of Arg^{mmm}-PG-1 in the POPE/POPG membrane. (a) S_{CH} of an ideal β -hairpin for various (τ , ρ) angles. The N- and C-strand S_{CH} 's are plotted as blue and red squares, respectively, with L5 and V14 values in black. The experimental C α S_{CH} 's for L5 and V14 in the POPE/POPG membrane are drawn as blue and red dashed lines, respectively. Some of the approximate best-fit orientations are highlighted in yellow to indicate the agreement with the experimental data. (b) RMSD between the calculated and experimental C α -H α order parameters of Arg^{mmm}-PG-1 in the POPE/POPG membrane as a function of (τ , ρ). (c) Topological structure of Arg^{mmm}-PG-1 in the POPE/POPG membrane.

To assess if the structure used in the S_{CH} calculation affects the orientation result significantly, we also calculated S_{CH} using the solution NMR structure of PG-1 (PDB: 1PG1)^[9]. In the 20 energy-minimized structures, the backbone conformations of the β -strand residues 5-9 and 12-17 have relatively small variations. We chose the representative structure #10 as the input for the orientation calculation. Fig. S6 shows that the best-fit τ angles fall in the same range as the ideal hairpin simulations, close to 90°, thus the conclusion that the strand axis is roughly parallel to the membrane plane is

unchanged. However, for the POPC/POPG membrane, even the best-fit (τ, ρ) angles of $(100^\circ, 152^\circ)$ does not agree with the experimental data very well (Fig. S6a), suggesting that the solution structure of PG-1 may deviate non-negligibly from the membrane-bound peptide structure. Nevertheless, the best-fit (τ, ρ) range of $(60^\circ\text{-}90^\circ, 150^\circ\text{-}180^\circ)$ is in general good agreement with the ideal hairpin simulations (Table S2). In conclusion, Arg^{mm}-PG-1 has the strand axis perpendicular to the membrane normal and has the hairpin plane roughly parallel to the membrane normal, regardless of the input structure.

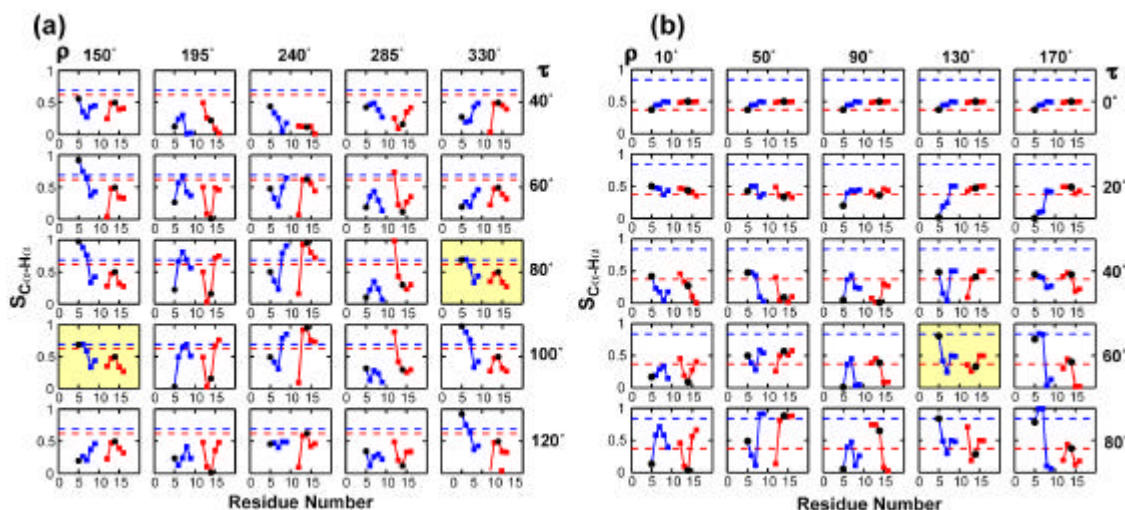


Fig. S6. Calculated S_{CH} 's using the PG-1 solution structure #10. Values of residues 5-9 and 12-17 are shown in blue and red squares, respectively, with the L5 and V14 S_{CH} 's in black. The experimental S_{CH} 's for L5 and V14 are drawn as blue and red dashed lines, respectively. (a) Experimental data is that of the POPC/POPG membrane. (b) Experimental data is that of the POPE/POPG membrane. The approximate best-fit orientations are highlighted in yellow to indicate the agreement with the experimental data.

The somewhat different quality of fit between the PG-1 solution NMR structure and the ideal β -hairpin structure can be explained by the distorted backbone conformation of the PG-1 solution structure, shown in Fig. S7. The $C\alpha$ - $H\alpha$ vectors are along the same direction in the ideal β -hairpin, but point to a range of directions in the solution NMR structure #10.

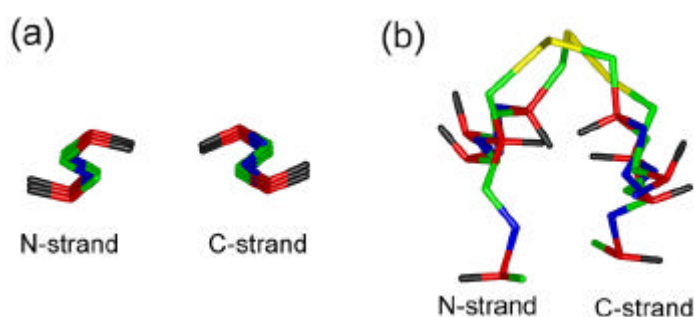


Fig. S7. Comparison of the structures of (a) the ideal β -hairpin and (b) PG-1 solution NMR structure #10 (PDB: 1PG1). $C\alpha$ and $H\alpha$ atoms are highlighted in red and black, respectively. The β -strand axis is perpendicular to the view plane. Residues 5-9 and 12-17 are shown in sticks.

Table S2 summarizes the best-fit orientations of Arg^{mm}-PG-1 in POPC/POPG and POPE/POPG membranes from simulations using the ideal β -hairpin structure and the solution NMR structure #10. The global best-fit angles in each case after taking into account the ^{13}C - ^{31}P distance constraints is listed in column A. All global best-fit orientations fall into a relatively narrow range of $(\tau, \rho) = (85\text{-}120^\circ, 130\text{-}180^\circ)$, indicating that Arg^{mm}-PG-1 strand axis is perpendicular to the bilayer normal. This is distinctively different from the transmembrane orientation of PG-1 [2].

Table S2. Best-fit (τ , ρ) angles for Arg^{mm}-PG-1 in POPC/POPG and POPE/POPG membranes. Solution A is the global best-fit based on agreement with the ^{13}C - ^{31}P distance constraints.

Structure	Membrane	A	B	C	D	Error
Ideal hairpin	POPC/POPG	(116°, 179°)	(64°, 359°)	(72°, 179°)	(108°, 359°)	$\pm 3^\circ$
Ideal hairpin	POPE/POPG	(113°, 164°)	(67°, 344°)	(76°, 164°)	(104°, 344°)	$\pm 3^\circ$
PG-1 #10	POPC/POPG	(100°, 152°)	(80°, 332°)	(46°, 153°)	(134°, 333°)	—
PG-1 #10	POPE/POPG	(89°, 137°)	(91°, 317°)	(60°, 133°)	(120°, 313°)	$\pm 6^\circ$

^1H spin diffusion

2D ^{31}P -detected ^1H spin-diffusion experiments were conducted at 303 K under 5 kHz MAS. After ^1H evolution, a mixing time (t_m) of 64 – 400 ms was applied to transfer ^1H polarization from the mobile lipids and water to the final destination of lipid headgroup ^{31}P for detection. In the absence of transmembrane proteins, the lipid chain CH_2 to ^{31}P cross peak is very slow to develop due to the extremely weak dipolar coupling. The presence of transmembrane peptides significantly facilitates the spin diffusion via the pathway $\text{CH}_2 \rightarrow \text{peptide} \rightarrow ^{31}\text{P}$. To ensure that only the mobile lipid and water polarization served as the source of spin diffusion, we suppressed the rigid peptide polarization by a ^1H T_2 relaxation filter of 0.8 ms before ^1H chemical-shift evolution and spin diffusion.

^{13}C - ^{31}P distance measurement

^{13}C - ^{31}P distances were measured using the rotational-echo double resonance (REDOR) experiment. Composite $90^\circ 180^\circ 90^\circ$ pulses were applied on the ^{31}P channel to

reduce the effect of flip angle errors and enhance the distance accuracy. At each REDOR mixing time (t_m), a control experiment (S_0) with the ^{31}P pulses off and a dephasing experiment (S) with the ^{31}P pulses on were carried out. The normalized dephasing, S/S_0 , as a function of t_m gives the ^{13}C - ^{31}P dipolar coupling. The ^{13}CO dephasing was corrected for the lipid natural-abundance CO contribution. The experiments were conducted under 4.5 kHz MAS at 225 K. ^{31}P 180° pulse lengths of 9 μs were used to achieve complete inversion of the broad ^{31}P resonance.

References

- [1] M. Tang, A. J. Waring, M. Hong, *J Am Chem Soc* **2005**, *127*, 13919.
- [2] R. Mani, S. D. Cady, M. Tang, A. J. Waring, R. I. Lehrer, M. Hong, *Proc. Natl. Acad. Sci. U.S.A.* **2006**, *103*, 16242.
- [3] B. J. vanRossum, C. P. deGroot, V. Ladizhansky, S. Vega, H. J. M. deGroot, *J. Am. Chem. Soc.* **2000**, *122*, 3465.
- [4] M. Munowitz, W. P. Aue, R. G. Griffin, *J. Chem. Phys.* **1982**, *77*, 1686.
- [5] J. C. C. Chan, R. Tycko, *J. Chem. Phys.* **2003**, *118*, 8378.
- [6] X. L. Yao, M. Hong, *J. Am. Chem. Soc.* **2002**, *124*, 2730.
- [7] H. Sun, L. K. Sanders, E. Oldfield, *J. Am. Chem. Soc.* **2002**, *124*, 5486.
- [8] M. Tang, A. J. Waring, R. I. Lehrer, M. Hong, *Biophys. J.* **2006**, *90*, 3616.
- [9] R. L. Fahrner, T. Dieckmann, S. S. Harwig, R. I. Lehrer, D. Eisenberg, J. Feigon, *Chem. & Biol.* **1996**, *3*, 543.